



Full length article

# Hybrid multi-objective robust design optimization of a truck cab considering fatigue life

Na Qiu <sup>a,b</sup>, Zhiyang Jin <sup>a,b,\*</sup>, Jinyi Liu <sup>a,b</sup>, Lirong Fu <sup>a</sup>, Zhenbin Chen <sup>a</sup>, Nam H. Kim <sup>c,\*</sup>

<sup>a</sup> Mechanical and Electrical Engineering College, Hainan University, Haikou, 570228, China

<sup>b</sup> Hainan Policy and Industrial Research Institute of Low-Carbon Economy, China

<sup>c</sup> Department of Mechanical & Aerospace Engineering, University of Florida, Gainesville, FL 32611, USA

## ARTICLE INFO

### Keywords:

Multi-objective robust design optimization  
Hybrid optimization  
Fatigue design  
Dual surrogate model  
Taguchi method  
Uncertainty

## ABSTRACT

Fatigue performance optimization without considering uncertainties of design variables can be problematic or even dangerous in real life. In this paper, a hybrid multi-objective robust design optimization methodology is proposed to make a proper tradeoff between the lightweight and fatigue durability for the design of a truck cab. However, the uncertainties, in reality, could lead to the optimized design unstable or even useless; this situation can be more serious in non-deterministic optimization. The Taguchi robust parametric design technique is adopted to refine the intervals of design variables for the subsequent optimization based on the validated simulation model against fatigue tests. Three types of dual surrogate models, namely the dual polynomial response surface, dual Kriging, and dual radial basis function methods are compared, and the dual Kriging is selected to model the mean and standard deviation of the mass and fatigue life for its high accuracy. The multi-objective particle swarm optimization algorithm is utilized to perform robust design. The Pareto fronts with different weight factors are analyzed to provide some insightful information on optimum designs. The robust optimization results demonstrate that the optimized design improves the fatigue life and reduces the mass of the truck cab significantly and becomes less sensitive to uncertainty. Different optimums can be obtained based on three different normalization techniques (Linear, vector, and LMM) and three MCDM methods (TOPSIS, WPM, and WSM) from the same Pareto front. The comparison analysis emphasizes the importance of normalization and MCDM method selection in the optimal design selection process.

## 1. Introduction

Fatigue life has drawn significant attention in a wide range of automotive industry due to its significant effect on the performance, safety, and durability of automobile structures. For example, Bayrakceken et al. [1] conducted the fatigue performance analysis of the drive shaft as well as the universal joint yoke of a vehicle power transmission. Colombo et al. [2] systematically investigated the failure causes of the strut seat on a suspension. Palma et al. [3] used the finite element analysis (FEA) method to evaluate fatigue performance for a trailer hook of a car. Veloso et al. [4] analyzed the failure performance of a stringer of a chassis system. He et al. [5] conducted the failure cause analysis of damper spring for a passenger car and estimated fatigue life.

Structural optimization techniques can be employed to improve the fatigue performance of vehicles. Hsu and Hsu [6] employed a sequential neural network method to perform the lightweight design of disk wheels with the constraints of fatigue life. Kang et al. [7] conducted the fatigue performance optimization of a lower control arm to ensure its durability. Mrzyglod and Zielinski [8] optimized

the parameters of a suspension arm based on the multi-axial fatigue criteria. Ping et al. [9] analyzed the fatigue performance of a vehicle body and optimized the spot weld to improve its durability. Adl and Panahi [10] improved the fatigue life-span and reduced the weight by performing a multi-objective optimization design for a car based on the artificial neural network method. Kaya et al. [11] presented a framework for a topology and shape optimization approach to re-design a failed component under cyclic loading. Kim et al. [12] optimized the outer tie rod of a passenger car to improve its durability. Song et al. [13] performed an optimization design of a control arm based on surrogate models to improve its strength and durability performance.

The above-mentioned studies on fatigue durability optimization are limited to deterministic design. However, in real-life, any design optimization may not afford to neglect uncertainty [14,15], which may pertain to material properties, manufacturing processes, and geometries, etc. It needs to be noticed that usually objective functions and constraints are conflicted with each other and the deterministic optimization tends to push the optimal design towards constraint

\* Corresponding authors.

E-mail addresses: [jinzhiyang94@163.com](mailto:jinzhiyang94@163.com) (Z. Jin), [nkim@ufl.edu](mailto:nkim@ufl.edu) (N.H. Kim).

boundaries, thereby leaving less room for manufacturing imperfections and/or tolerances. To overcome this limitation, some researchers have developed reliability-based design optimization (RBDO). For example, Boessio et al. [16] estimated the fatigue lifetime of a vehicle considering the presence of random rough pavement surfaces and optimized the structural design with the constraints of the reliability index. d'Ippolito et al. applied RBDO of fatigue life to a slat-track considering manufacturing tolerances of geometric parameters [17]. They also employed this method to optimized structures of a vehicle knuckle including the effect of variability in material parameters [18]. Song and Lee [19] utilized a constraint-feasible moving least-squares approach to perform the RBDO for a knuckle component.

In addition to the reliability of structural fatigue, robustness has been another critical issue in optimization with uncertainties. This is because when optimization searches for a "peak" solution, sometimes a subtle perturbation in system parameters and/or design variables could lead to a substantial change of performance, even result in a misleading "optimized design". Although RBDO helps to obtain a reliability optimum within constraints, it does not directly deal with uncertainty in design. The robust design optimization (RDO) aims to address this critical issue by controlling uncertainty, to guarantee the quality of optimal design [14,15]. The concept of robust design was established by Genichi Taguchi to made the product less sensitive to the uncontrolled real-life variations of variables and thus improve the quality of manufactured goods. This issue has drawn some attention in the literature [20–23]. Zhou et al. [24] found that the prediction uncertainty from the surrogate models has a more serious effect on the robust optimization results. However, limited studies have been found on RDO for structural fatigue in the automotive industry to date [25].

To meet today's design requirements and improve the fuel efficiency of vehicles, there is an increasing demand for assuring the lightweight of vehicle components. However, many performance indices are typically employed to characterize engineering problems in real-life, some of which (e.g. fatigue durability) could conflict with the lightweight requirement. Thereby, an appropriate compromise between the mass and other performance indices should be made. Multi-objective optimization has proven to be one of the most effective tools for this purpose [14,15]. Multi-objective optimization typically leads to a Pareto front amongst a range of conflicting objectives, not just a unique optimal solution, thereby providing decision-makers with more insightful data for design justification [26–28].

Although design under uncertainty has been explored extensively, its industrial applications anticipated a lot of challenges, including impractically high computational cost, inaccuracy of surrogate models to estimate the level of uncertainty, exploring multiple objectives (goals) in high-dimensional parameter space, and exploring multiple optimums. The current manuscript has two contributions for overcoming the abovementioned challenges. First, we present a practical case study of robust design optimization of fatigue life and lightweight. Such a seemingly simple problem still requires many practical considerations for engineers to obtain acceptable design, such as exploring parameter design using the Taguchi method, and building dual surrogate models, and solving a multi-objective optimization problem. Therefore, this manuscript can be a good case study for engineers in practice. The second contribution is related to the fact that engineers often obtain multiple optimum designs and need to make a decision among them. In this manuscript, it is shown that different optimums can be obtained based on three multi-criteria decision-making (MCDM) methods (TOPSIS, WPM, and WSM) and three different normalization schemes (Linear, vector, and LMM) from the same Pareto front. This topic has significant scientific research values and needs to be further studied.

In this paper, to address a fatigue optimization problem of a truck cab with consideration of the uncertainties on material properties, a hybrid multi-objective robust optimization (MORDO) procedure was proposed in Section 2. In Section 3, the dual surrogate model and Taguchi parameter design with a multi-objective MOPSO algorithm

**Table 1**  
Expressions of S/N ratio.

Quality characteristics	Expression
Lower-the-better	$S/N = -10 \log(\frac{1}{n} \sum y_i^2)$
Larger-the-better	$S/N = -10 \log(\frac{1}{n} \sum \frac{1}{y_i^2})$
Nominal-the-better	$S/N = 10 \log(\frac{\mu^2}{\sigma^2}), \mu = \frac{1}{n} \sum y_i, \sigma^2 = \frac{1}{n-1} \sum (y_i - \mu)^2$

were integrated. The Taguchi parameter design approach is used to help better initialize the design space for the subsequent surrogate-based optimization. After the sizes and dimensions of the design space are explored, different dual surrogate models are constructed to fit both the mean and standard deviation of the mass and fatigue objectives of the truck cab. Based on the achieved accuracy, the dual Kriging model is selected to perform the subsequent optimization. Finally, MOPSO is adopted to solve the MORDO problem for seeking a robust Pareto front in Section 4. To achieve the best final design, different MCDM methods and different normalization techniques are implemented for the same Pareto front.

## 2. Hybrid multi-objective robust design optimization

### 2.1. Parameter design of Taguchi method

Taguchi method is a statistical method aiming to improve the quality of manufactured goods, which is developed by Genichi Taguchi. Nowadays, the Taguchi method has been applied successfully to solving many engineering problems [29,30]. In this regard, Taguchi assumed that engineering optimization should be conducted through the following procedure [31]; i.e., system design, parameter design, and tolerance design. The objective of parameter design is to optimize the setting of parameters to improve system performance. Besides, the optimal parameters should be insensitive to the involved noise factors.

The Taguchi method uses an orthogonal array as a statistical approach to explore the effects of multiple variables simultaneously, with a relatively small number of experiments compared to the classical design of experiments methods. The experimental results are then transformed into a signal-to-noise (S/N) ratio as a combined measure of the mean and standard deviation of the quality characteristic. Taguchi classifies the parametric design problem into three categories based on the quality characteristics of output ( $y_i$ ); i.e., lower-the-better, larger-the-better, and nominal-the-better; and their S/N ratios are given in Table 1.

A higher S/N ratio indicates a better-quality characteristic. Thus, the level with the highest S/N ratio is the optimal level of the parameters. In this study, the Taguchi parametric design is used to reduce the dimension and size of the design space as suggested in the literature [32,33]. Moreover, the refinement of design space can enhance the accuracy of subsequent surrogate modeling because it is commonly acknowledged that a smaller region can achieve a higher accuracy [34].

### 2.2. Multi-objective robust design optimization

For an uncertainty case, robust design optimization takes into account the uncertainty factors, aiming to enhance the nominal performances of the objectives while reducing the variability of the performances. Typically, a multi-objective robust design optimization (MORDO) problem can be formulated as

$$\begin{cases} \min \{ f_1(Y_{\mu_1}(\mathbf{x}), Y_{\sigma_1}(\mathbf{x})), \dots, f_i(Y_{\mu_i}(\mathbf{x}), Y_{\sigma_i}(\mathbf{x})) \} \quad i = 1, 2, \dots, m \\ \text{s.t. } g_j(\mathbf{x}) \leq 0 \quad j = 1, 2, \dots, n \\ \mathbf{x}^L \leq \mathbf{x} \leq \mathbf{x}^U \end{cases} \quad (1)$$

where  $Y_{\mu_i}(\mathbf{x})$  and  $Y_{\sigma_i}(\mathbf{x})$  denotes the mean and standard deviation of the  $i$ th objective, respectively. It is also possible that uncertainty can affect constraints. Since the uncertainties in constraints are not important

**Table 2**

Expression of the weighted objective function including the mean and standard deviation.

Objective type	Expression
Minimization	$f_i(Y_{\mu}(\mathbf{x}), Y_{\sigma}(\mathbf{x})) = \lambda Y_{\mu}(\mathbf{x}) + (1 - \lambda) Y_{\sigma}(\mathbf{x})$
Maximization	$f_i(Y_{\mu}(\mathbf{x}), Y_{\sigma}(\mathbf{x})) = -\lambda Y_{\mu}(\mathbf{x}) + (1 - \lambda) Y_{\sigma}(\mathbf{x})$

as long as the constraints are satisfied, reliability-based optimization is used for the constraints with uncertainty. When the reliabilities of constraints are considered, the problem formulation is called reliability-based robust optimization [35–37]. Since the reliability constraint can be handled separately from robustness, it is considered as out of the scope of the current study.

The objective vector in Eq. (1) can be rewritten weighted sum form as shown in Table 2, where  $\lambda$  is the weight factor to emphasize their relative importance.

### 2.3. Dual surrogate model (DSM)

In engineering optimization, direct performing optimization based on the simulation model can be very difficult (if not impossible) since iterative simulations require high computational costs [38] and may not converge. As an alternative, the surrogate modeling technique appears effective for many complicated problems. It builds an approximate function to formulate responses in terms of design variables with a moderate number of simulations. Once the surrogate model is accurate enough to approximate the responses, it can replace simulation to run the optimization.

Response surface methodology is one of the most widely used surrogate modeling techniques. The classical polynomial response surface usually emphasizes the mean value of responses without considering uncertain parameters. However, the polynomial response surface may not be adequate under uncertainty and the optimization could become even meaningless [39]. To solve this issue, the dual polynomial response surface (DPRS) was utilized to simultaneously models the mean and standard deviation as Eqs. (2)–(3). In this study, a second-order of polynomials is used for DPRS. This approach has been adopted for robust design in the literature [39–43].

$$\hat{Y}_{\mu}(\mathbf{x}) = b_0 + \sum_{i=1}^k b_i x_i + \sum_{i=1}^k b_{ii} x_i^2 + \sum_{i < j}^k b_{ij} x_i x_j \quad (2)$$

$$\hat{Y}_{\sigma}(\mathbf{x}) = c_0 + \sum_{i=1}^k c_i x_i + \sum_{i=1}^k c_{ii} x_i^2 + \sum_{i < j}^k c_{ij} x_i x_j \quad (3)$$

The specific steps to fit the dual polynomial response surface can be summarized as follow:

- (1) Construct the cross-product array using the Taguchi method;
- (2) Capture the variability by repeating the numerical experiments over the uncertain (noise) range of parameters;
- (3) Extract the mean and standard deviation at all design samples;
- (4) Build response surfaces for both the mean and standard deviation;
- (5) Check for accuracy of the dual response surface models;
- (6) Repeat the above steps until obtaining the acceptable accuracy.

The polynomial response surface is relatively simple to derive parameter sensitivity, but might be unsatisfactory sometimes, in particular for highly nonlinear problems [44]. To address the issue of model form error, other surrogate models are commonly used in solving complicated optimization problems, for example, Kriging models and radial basis function [45–52]. In this paper, we construct the dual polynomial response surface using the following surrogate models, in which Eqs. (4) and (5) are used for the dual Kriging (DKRG) model, and Eqs. (6) and (7) are used for the dual radial basis function (RBF) model, respectively. For Kriging, what was the trend function is linear

and the hyperparameters are estimated by the maximum likelihood function. The basic functions for RBF surrogate models are multi-quadratic functions (specifically  $\phi(r) = \sqrt{r^2 + c^2}$  and  $c$  is the free shape parameter [53]). The polynomial term  $P$  of the RBF model is not used. They are the same for mean and standard deviation.

$$\hat{Y}_{\mu}(\mathbf{x}) = \hat{\beta}_{\mu} + \mathbf{r}_{\mu}^T(\mathbf{x}) \mathbf{R}_{\mu}^{-1}(\mathbf{y}_{\mu} - \mathbf{f}_{\mu} \hat{\beta}_{\mu}) \quad (4)$$

$$\hat{Y}_{\sigma}(\mathbf{x}) = \hat{\beta}_{\sigma} + \mathbf{r}_{\sigma}^T(\mathbf{x}) \mathbf{R}_{\sigma}^{-1}(\mathbf{y}_{\sigma} - \mathbf{f}_{\sigma} \hat{\beta}_{\sigma}) \quad (5)$$

$$\hat{Y}_{\mu}(\mathbf{x}) = \sum_{j=1}^m c_{\mu j} p_{\mu j}(\mathbf{x}) + \sum_{i=1}^{n_s} \lambda_{\mu i} \phi_{\mu}(r_{\mu}(\mathbf{x}, \mathbf{x}_i)) \quad (6)$$

$$\hat{Y}_{\sigma}(\mathbf{x}) = \sum_{j=1}^m c_{\sigma j} p_{\sigma j}(\mathbf{x}) + \sum_{i=1}^{n_s} \lambda_{\sigma i} \phi_{\sigma}(r_{\sigma}(\mathbf{x}, \mathbf{x}_i)) \quad (7)$$

Through a comparative study, the model with the highest accuracy will be selected to replace simulations in optimization herein. Because good accuracy for surrogate models does not mean a good fit for optimization [54,55], the accuracy of optimal design will be checked with their simulation results as shown in Fig. 1. To evaluate the accuracy of the surrogate model, three metrics are utilized to evaluate the accuracy, namely R-square, relative average absolute error (RAAE), and relative maximum absolute error (RMAE) [44,56,57]. In general, a large value of  $R^2$  and a small value of RAAE indicate a high global accuracy in the design space and thus are preferred. On the other hand, a small value of RMAE is preferred, which indicates a high local accuracy in some regions of the design space. In practice, we mainly pay attention to global accuracy and thus place more emphasis on the first two metrics.

### 2.4. Multi-objective particle swarm optimization algorithm

Once the dual surrogate model is available, it can be used to solve the multi-objective robust optimization problem. MOPSO algorithm is an extended version of the particle swarm optimization algorithm [58], which is a well-established metaheuristic algorithm. Compared with other multi-objective optimization algorithms such as PEAS, NSGA-II [59,60], and micro PGA [61–63], MOPSO has the properties of well-distributed Pareto front and fast convergence. MOPSO has been used successfully in various engineering applications [64–70] to optimize the design of metal sheet forming [57] and crashworthiness for thin-walled structures [71], and thus is also employed in this study. More details are given in Ref. [62].

The proposed hybrid multi-objective robust optimization (MORDO) methodology is illustrated in Fig. 1. It uses the Taguchi method first to explore the design and parameter spaces and to reduce the dimensions. Besides, it will also reduce the range of design space. Then, the dual surrogate model is constructed using the inner and outer arrays from the Taguchi method. This step is repeated until the accuracy of the dual surrogate model is acceptable. Once the dual surrogate model is available, the MOPSO algorithm is invoked to calculate the Pareto fronts for multiple objective functions. This sequential optimization design method can perform better than the traditional approach in obtaining better optimums based on fewer samples. Because for the sequential optimization design, only limited evaluations are required in each iteration, but the accuracy can be improved a lot.

## 3. Demonstrative example of fatigue optimization for a truck cab

### 3.1. Finite element model building and experimental validation

The 3D geometry of the cab-in-white model and the corresponding finite element FE (FE) model is illustrated in Fig. 2. For such a complicated 3D model, validation is needed before the design study. In this regard, modal analysis is a useful validation approach, which can be performed with a free-free boundary to calculate the cab's natural frequency before running stress analysis. If the first six zero rigid body modes cannot confirm, the FE model could be over-constrained.

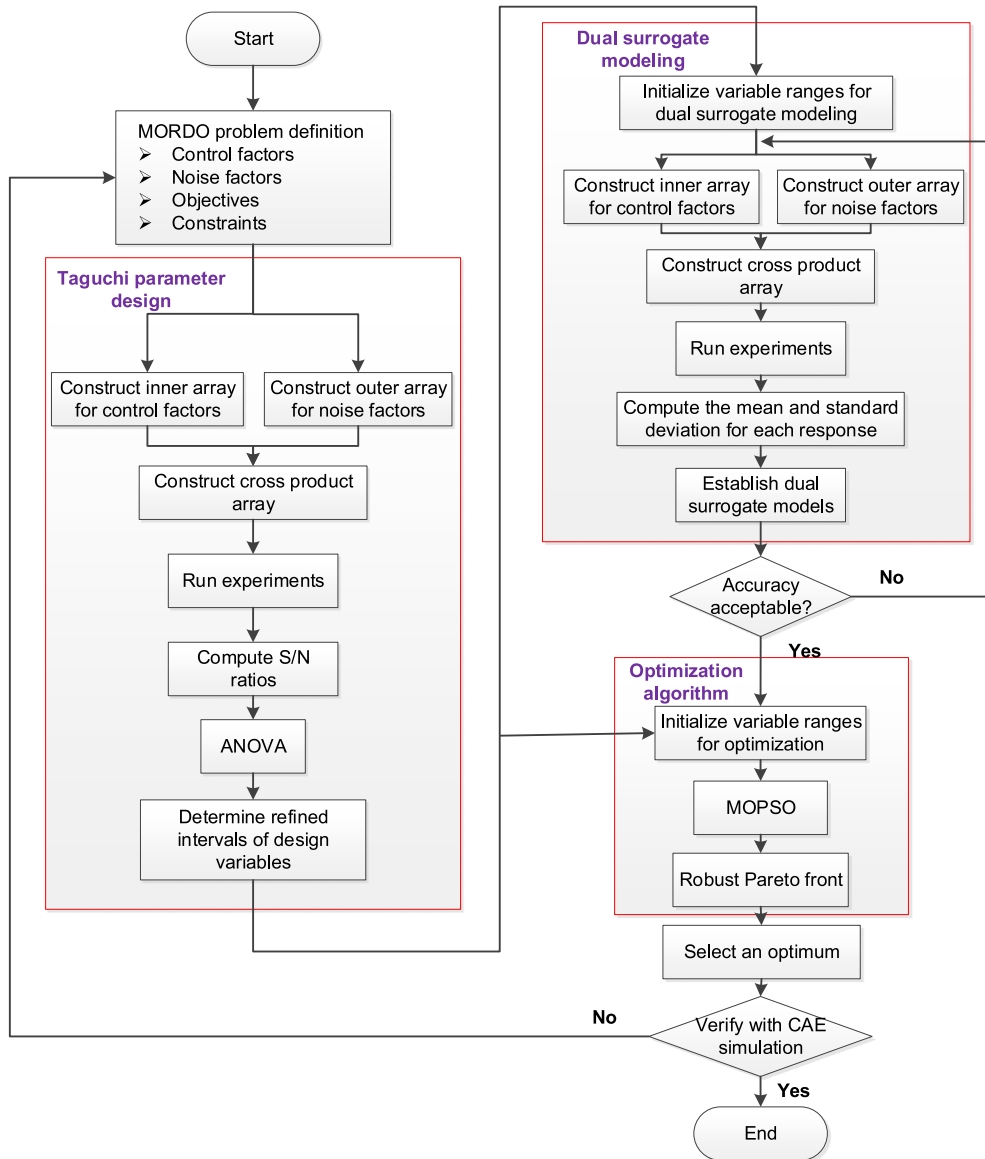


Fig. 1. Flowchart of the proposed hybrid methodology for MORDO.

However, if zero rigid body modes are more than six, the FE model could have ruptured. In addition to the modal test, the full-scale fatigue test is also performed to validate the fatigue life prediction.

In this study, the durability prediction method is employed based on direct transient response. MSC-Nastran is utilized to get the stress history of each element, based on the input of load-time history. When the front body mounts are fixed, the cab is subjected to a torsional cyclic moment at the rear body mounts. As shown in Fig. 2b,  $F_1$  and  $F_2$  generate the torsional moment, and its frequency and amplitude are set as 1 Hz and 5000 Nm [72], respectively.

To obtain durability performance, the stress response history is used directly in the MSC Fatigue module. Strain-life methods of durability prediction with transient analysis can be utilized in this case. The strain-life ( $\epsilon$ -N) curve is represented by the classical Coffin–Manson equation, as shown in the following equation [73,74]:

$$\frac{\Delta\epsilon}{2} = \frac{\Delta\epsilon_e}{2} + \frac{\Delta\epsilon_p}{2} = \frac{\sigma'_f}{E}(2N_f)^b + \epsilon'_f(2N_f)^c \quad (8)$$

where  $\Delta\epsilon/2$  are total strain amplitudes,  $\Delta\epsilon_e/2$  and  $\Delta\epsilon_p/2$  denotes elastic and plastic strain amplitudes, respectively.  $\sigma'_f$  and  $b$  are fatigue strength

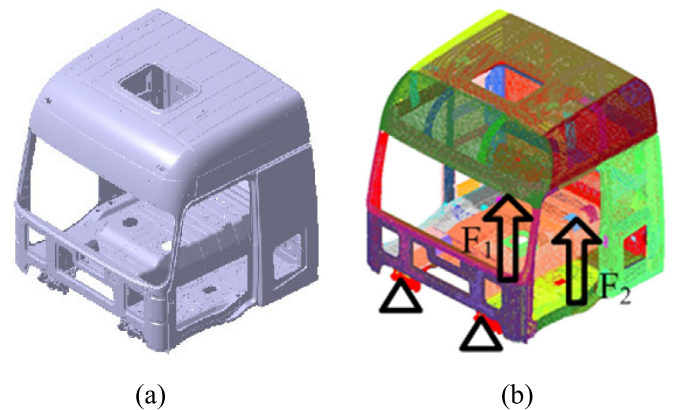


Fig. 2. Truck cab model: (a) 3D geometric model and (b) finite element model.

and fatigue strength exponent, respectively.  $\epsilon'_f$  and  $c$  are fatigue ductility coefficient and fatigue ductility exponent, respectively. These

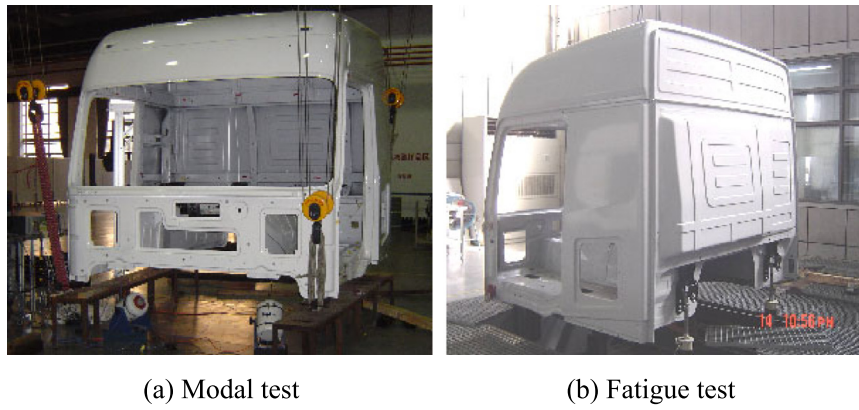


Fig. 3. Experimental tests.

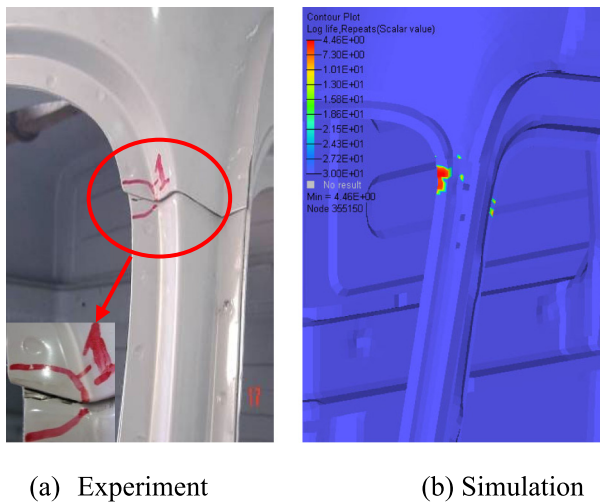


Fig. 4. Comparison of experimental data and numerical simulation for fatigue durability.

Table 3  
Validation of the FE model: comparison between simulation and experimental results.

	Simulation	Experiment
Torsional frequency	20.06 Hz	19.94 Hz
Bending frequency	29.64 Hz	28.47 Hz
Log of fatigue life	4.46	4.60

parameters can be derived from the Bäumel–Seeger’s uniform material law [75], which can be easy to obtain based on the ultimate tensile strength ( $\sigma_b$ ) and elastic modulus ( $E$ ) of material.

The finite element model describing the structural behavior of the truck cab was validated by comparing it with experimental data. Fig. 3 demonstrates the setup of physical tests with the same loading conditions as in the simulations. As shown in Table 3, the simulation results agree well with the corresponding experimental results. Fig. 4 shows that the weakest regions of fatigue durability are identical between the experiment and the simulation. Hence, the FE models are validated and considered effective for the subsequent design optimization.

### 3.2. Definition of the optimization problem

Vehicle weight reduction can bring many benefits, including using fewer materials, less fuel consumption, less exhaust emission, and less non-biodegradable materials. Unfortunately, the automotive industry’s demand for reducing weight inevitably conflicts with other design

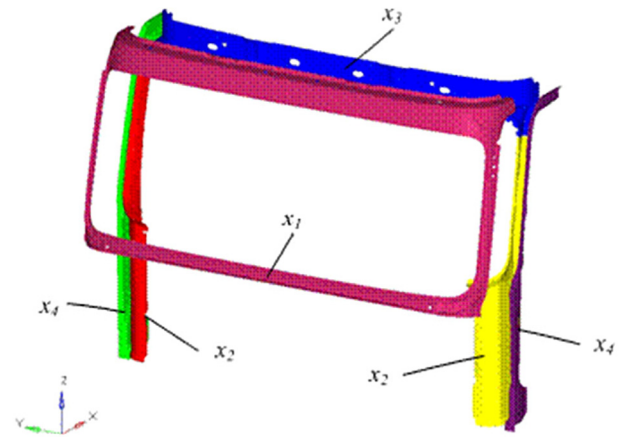


Fig. 5. Thickness design variables.

criteria such as the overall strength, stiffness, safety durability, and corrosion resistance of the body. In this paper, the maximization of fatigue life and minimization of lightweight are chosen as two competing objectives to be optimized within a multi-objective framework. Considering symmetry, four thicknesses of six panels were chosen as the design variables for cab structural optimization. As shown in Fig. 5,  $x_1$  is the thickness of the window frame,  $x_2$  is the thickness of the A-pillar inner plate,  $x_3$  is the thickness of the roof Crossrail and  $x_4$  is the thickness of the A-pillar outer plate. All the thickness design variables are allowed to vary from 0.7 to 2.0 mm.

Considering the uncertainty induced by the rolling process, the key material properties are chosen as noise factors. To be specific, their fluctuated range are  $E = (200, 220 \text{ GPa})$ ,  $\sigma_b = (300, 340 \text{ MPa})$ , and  $\rho = (7700, 7900 \text{ kg/m}^3)$  according to the statistical data in the literature [76]. The MORDO problem can be expressed as:

$$\begin{cases} \min (f_1(\mathbf{x}), f_2(\mathbf{x})) \\ f_1(\mathbf{x}) = -\lambda F_\mu + (1 - \lambda)F_\sigma \\ f_2(\mathbf{x}) = \lambda M_\mu + (1 - \lambda)M_\sigma \\ \text{s.t. } \mathbf{x}_L \leq \mathbf{x} \leq \mathbf{x}_U \end{cases} \quad (9)$$

where  $F_\mu$  is the mean of the log of fatigue life and  $F_\sigma$  denotes the standard deviation of the log of fatigue life,  $M_\mu$  is the mean of the masses of the six panels and  $M_\sigma$  is the standard deviation of the masses of the six panels (Fig. 5).

**Table 4**  
Cross product array for parameter design.

No	$x_1$	$x_2$	$x_3$	$x_4$	$E$		$\rho$		$\sigma_b$		$F$		$M$		$S/N_1$	$S/N_2$
					-1	+1	-1	+1	-1	+1	F	M	F	M		
1	1	1	1	1	3.07	15.41	3.18	15.82	3.24	15.41	3.19	15.82	3.18	15.61	0.61	29.14
2	1	2	2	2	3.31	19.67	3.41	20.18	3.49	19.67	3.44	20.18	3.43	19.92	0.74	27.02
3	1	3	3	3	3.40	26.75	3.51	27.45	3.40	26.75	3.36	27.45	3.43	27.10	0.74	24.35
4	1	4	4	4	3.43	33.84	3.54	34.72	3.48	33.84	3.44	34.72	3.48	34.28	0.76	22.31
5	2	1	2	3	3.47	23.32	3.59	23.93	3.49	23.32	3.45	23.93	3.51	23.62	0.78	25.54
6	2	2	1	4	3.68	26.06	3.82	26.74	3.73	26.06	3.67	26.74	3.73	26.40	0.89	24.58
7	2	3	4	1	3.87	26.99	4.02	27.69	3.89	26.99	3.82	27.69	3.91	27.34	0.97	24.27
8	2	4	3	2	3.88	28.72	4.03	29.46	3.92	28.72	3.86	29.46	3.93	29.09	0.98	23.74
9	3	1	3	4	3.75	32.06	3.87	32.89	3.86	32.06	3.80	32.89	3.83	32.48	0.93	22.78
10	3	2	4	3	4.22	32.91	4.37	33.76	4.36	32.91	4.27	33.76	4.32	33.33	1.14	22.55
11	3	3	1	2	4.34	26.93	4.53	27.63	4.43	26.93	4.32	27.63	4.41	27.28	1.18	24.29
12	3	4	2	1	4.37	28.89	4.56	29.64	4.44	28.89	4.33	29.64	4.43	29.27	1.19	23.68
13	4	1	4	2	4.14	32.80	4.28	33.65	4.28	32.80	4.19	33.65	4.23	33.23	1.10	22.58
14	4	2	3	1	4.73	30.42	4.93	31.21	4.90	30.42	4.76	31.21	4.84	30.81	1.34	23.24
15	4	3	2	4	4.97	37.47	5.22	38.44	5.25	37.47	5.04	38.44	5.12	37.96	1.44	21.42
16	4	4	1	3	4.82	35.79	5.05	36.72	5.04	35.79	4.85	36.72	4.95	36.25	1.38	21.82

**Table 5**  
Values of the noise factors for parameter design.

Code	$E$ (GPa)	$\rho$ (kg/m <sup>3</sup> )	$\sigma_b$ (MPa)
-1	200	7700	300
+1	220	7900	340
0	210	7800	320

## 4. Results and discussion

### 4.1. Parameter design

In this paper, the initial intervals of design variables are determined by the Taguchi method and the matrix of experiments are built by the orthogonal arrays. As shown in Table 4, the inner array concerning four design variables at four levels each is chosen as the L16 matrix, while the inner array concerning the three noise factors is also established based upon the orthogonal array. Tables 5 and 6 represent the value of the design variables and control factors that are used in the inner and outer arrays. Since each set of design variables has five combinations of noise array, a total of 80 experiments should be conducted. After numerical experiments are done, S/N ratios for the experiments are computed for the fatigue life ( $S/N_1$ ) and mass ( $S/N_2$ ), which are shown in the last column of Table 4.

Analysis of variance (ANOVA) is conducted from the S/N ratios, which are utilized to represent the relative importance of various factors. ANOVA of the fatigue life and the truck cab mass are shown in Tables 7 and 8, respectively. The optimal set of design variables is selected based on the ANOVA analyses. Level 1 is the best for all design variables with respect to the mass objective because high values of S/N are preferred. It can be seen that  $x_1$  has the most important effect on both objectives, with a contribution of 85.46% and 45.29%, respectively. Since Level 4 is selected for the fatigue life objective, the range of  $x_1$  is determined without any change as level-1 <  $x_1$  < level-4.  $x_4$  has a weak contribution to the fatigue life objective and level 1 is also preferred for that, and the value can be  $x_4 = 0.7$  mm. The ranges of  $x_2$  and  $x_3$  can be determined using the same method, and the results of parameter design are summarized in Table 9.

### 4.2. Dual surrogate models

After the refinement of variable ranges, dual surrogate models can be constructed in terms of  $x_1$ ,  $x_2$ , and  $x_3$  since  $x_4$  has been fixed at 0.7 mm as shown in Section 4.1. The outer array is the noise factors obtained from the orthogonal array as shown in Table 10. The inner array is control factors with 30 sample points, which are sampled

**Table 6**  
Values of the design variables for parameter design.

Level	$x_1$ (mm)	$x_2$ (mm)	$x_3$ (mm)	$x_4$ (mm)
1	0.7	0.7	0.7	0.7
2	1.0	1.0	1.0	1.0
3	1.5	1.5	1.5	1.5
4	2.0	2.0	2.0	2.0

**Table 7**  
ANOVA of the fatigue life.

	$x_1$	$x_2$	$x_3$	$x_4$
Level1	0.7113	0.8560	1.0118	<b>1.0239</b>
Level2	0.9020	1.0245	<b>1.0348</b>	0.9984
Level3	1.1084	<b>1.0798</b>	0.9958	1.0085
Level4	<b>1.3143</b>	1.0756	0.9935	1.0051
SS	0.8127	0.1325	0.0044	0.0014
Contribution	85.46%	13.93%	0.46%	0.15%

**Table 8**  
ANOVA of the truck cab mass.

	$x_1$	$x_2$	$x_3$	$x_4$
Level1	<b>25.7054</b>	<b>25.0102</b>	<b>24.9583</b>	<b>25.0826</b>
Level2	24.5322	24.3472	24.4180	24.4082
Level3	23.3268	23.5852	23.5250	23.5669
Level4	22.2656	22.8874	22.9287	22.7724
SS	26.5823	10.1753	9.8371	12.1047
Contribution	45.29%	17.33%	16.76%	20.62%

**Table 9**  
Results of parameter design: bounds of design variables.

Design variables	Varying ranges	
	Lower bound	Upper bound
$x_1$ (mm)	0.7	2.0
$x_2$ (mm)	0.7	1.5
$x_3$ (mm)	0.7	1.0
$x_4$ (mm)	0.7	0.7

with the Optimal Latin Hypercube sampling approach [14,15,77]. Additional five points of control factors are generated for assessing the accuracy of the surrogate models. To capture the variability due to the uncertainties of noise factors, numerical experiments in the inner array are repeated at five points corresponding to the outer array. Hence, the total simulation number is 175. The mean and standard deviation of each design are displayed in Table 11.

Because the mass of the cab has a linear relationship with the panel thicknesses, the dual linear polynomial response surfaces are utilized

**Table 10**  
Cross product array for DSMs.

No.	$x_1$	$x_2$	$x_3$	$E$		$\rho$		$\sigma_b$		$F$		$M$	
				$-1$	$-1$	$1$	$1$	$0$	$0$	$0$	$0$	$0$	$0$
1	1.69	0.76	0.95	4.07	24.47	4.21	25.11	4.13	24.47	4.06	25.11	4.13	24.79
2	1.96	1.31	0.82	4.65	28.56	4.87	29.30	4.82	28.56	4.66	29.30	4.75	28.93
3	1.91	1.11	0.97	4.63	27.95	4.85	28.67	4.81	27.95	4.65	28.67	4.74	28.31
4	1.60	1.22	0.91	4.47	25.72	4.67	26.39	4.56	25.72	4.44	26.39	4.54	26.06
5	1.10	0.98	0.83	4.09	20.41	4.26	20.94	4.07	20.41	4.00	20.94	4.12	20.68
6	0.97	0.73	0.88	3.63	18.41	3.74	18.88	3.75	18.41	3.71	18.88	3.76	18.65
7	1.87	1.17	0.73	4.54	26.83	4.75	27.52	4.68	26.83	4.54	27.52	4.63	27.17
8	0.74	1.25	0.80	3.32	18.72	3.42	19.21	3.50	18.72	3.44	19.21	3.43	18.96
9	1.37	1.14	0.79	4.28	23.10	4.46	23.70	4.30	23.10	4.21	23.70	4.32	23.40
10	1.82	0.81	0.77	4.25	25.02	4.41	25.67	4.33	25.02	4.24	25.67	4.32	25.35
11	1.15	1.33	0.87	4.11	22.53	4.28	23.11	4.09	22.53	4.02	23.11	4.13	22.82
12	0.92	1.09	0.72	3.66	19.02	3.78	19.51	3.87	19.02	3.80	19.51	3.79	19.27
13	1.33	1.36	0.99	4.19	24.59	4.37	25.23	4.23	24.59	4.14	25.23	4.24	24.91
14	1.46	1.00	1.00	4.32	24.06	4.51	24.69	4.39	24.06	4.29	24.69	4.38	24.38
15	1.06	1.20	0.96	4.03	21.60	4.18	22.16	4.01	21.60	3.94	22.16	4.05	21.88
16	0.79	0.87	0.78	3.35	17.23	3.46	17.67	3.55	17.23	3.48	17.67	3.47	17.45
17	1.73	1.03	0.86	4.48	25.68	4.69	26.34	4.61	25.68	4.47	26.34	4.57	26.01
18	0.70	1.06	0.90	3.22	17.89	3.32	18.35	3.40	17.89	3.34	18.35	3.34	18.12
19	1.19	0.78	0.74	3.98	19.84	4.12	20.35	3.96	19.84	3.91	20.35	4.00	20.10
20	1.42	1.50	0.84	4.30	25.30	4.49	25.96	4.34	25.30	4.25	25.96	4.35	25.63
21	0.88	0.92	0.98	3.67	19.03	3.78	19.52	3.85	19.03	3.78	19.52	3.80	19.27
22	1.51	0.70	0.81	3.91	22.23	4.04	22.81	3.93	22.23	3.87	22.81	3.95	22.52
23	0.83	1.42	0.93	3.59	20.71	3.69	21.25	3.79	20.71	3.72	21.25	3.71	20.98
24	1.64	1.39	0.75	4.48	26.16	4.68	26.84	4.57	26.16	4.44	26.84	4.55	26.50
25	2.00	0.89	0.89	4.49	27.29	4.67	28.00	4.61	27.29	4.50	28.00	4.58	27.65
26	1.55	0.95	0.71	4.36	23.27	4.56	23.88	4.42	23.27	4.31	23.88	4.42	23.57
27	1.78	1.44	0.94	4.60	28.26	4.82	29.00	4.75	28.26	4.60	29.00	4.70	28.63
28	1.28	0.84	0.92	4.06	21.55	4.21	22.11	4.08	21.55	4.01	22.11	4.10	21.83
29	1.24	1.28	0.70	4.21	22.27	4.39	22.85	4.20	22.27	4.12	22.85	4.24	22.56
30	1.01	1.47	0.76	3.90	21.66	4.02	22.22	4.03	21.66	3.97	22.22	4.03	21.94
31	2.00	1.30	1.00	4.73	29.63	4.96	30.40	4.95	29.63	4.76	30.40	4.85	30.02
32	1.35	0.70	0.93	3.82	21.48	3.96	22.04	3.84	21.48	3.78	22.04	3.86	21.76
33	1.03	1.50	0.85	3.96	22.25	4.09	22.82	4.03	22.25	3.97	22.82	4.07	22.54
34	1.68	1.10	0.70	4.43	24.88	4.63	25.53	4.52	24.88	4.40	25.53	4.50	25.21
35	0.70	0.90	0.78	3.13	16.65	3.24	17.08	3.31	16.65	3.25	17.08	3.25	16.86

to model both the mean and standard deviation of the mass. Detailed parameters for each surrogate model can be found in Section 2.3. For the fatigue life, different surrogate models are compared for determining the modeling accuracy. According to the results of the accuracy assessment shown in Table 12, the DKRG model performs best in accuracy and thus is selected for the following optimization procedure.

4.3. Optimization results and discussions

Fig. 6 plots the optimal Pareto fronts of robust multi-objective optimizations with different values of  $\lambda$ . For the Pareto fronts, the population size is set as 100 and the number of generations is 100 too. For MOPSO, the Maximum Number of Iterations is set as 100, grid inflation parameter is set as 0.1, Number of Grids per each dimension is 10, leader Selection Pressure Parameter is 4, and repository member selection pressure is 2. The Pareto solutions for different values of  $\lambda$  represent optimums in different cases. For example, when  $\lambda = 1.00$  (variance term equals zero as in Eq. (8)), the Pareto front represents the deterministic solution, which shows that the mean values of the mass and fatigue life (Fig. 6a) are strongly competing with each other. Consequently, if the mass is emphasized more, fatigue life must be compromised and become shorter, and vice versa. Interestingly, however, the standard deviations do not conflict with each other as shown in Fig. 6b. For example, when  $\lambda = 0.5$  (mean term and variance term are equally important as in Eq. (8)), the standard deviation of fatigue performance are the first decreased, increased, decreased, increase, and then decreased with the increase of standard deviation of mass. This may be because the mean's order of magnitude is much larger than the one of standard deviation. When  $\lambda$  is not small (for example  $\lambda > 0.01$ ), the mean value plays a dominant role due to its large magnitude and

big weight factors. Thus the standard deviation does not demonstrate conflict property. But when  $\lambda$  is very small (for example  $\lambda = 0.01$ ), the standard deviation is emphasized and it shows some conflict between the standard deviation of fatigue and mass.

Most importantly, when the uncertainties of the material properties are considered, the Pareto front changes evidently for both the mean and standard deviation (as shown in Fig. 7), and the change with the decreasing  $\lambda$  can be divided into three stages. First, when much emphasis is placed on the mean (i.e.,  $0.10 < \lambda < 1.00$ ), the Pareto fronts of MORDO indeed emerge as part of the deterministic Pareto front ( $\lambda = 1.00$ ). At this stage, when considering the objective robustness, the optima of deterministic multi-objective optimization located in the region representing the largest mass (i.e. in the upper left corner in Fig. 6a) fail to become candidate optima for MORDO, because these optima have the lowest mass robustness (in the upper right corner in Fig. 6b), although they can lead to the best fatigue performance.

Second, when  $\lambda$  has an intermediate value ( $0.01 < \lambda < 0.10$ ), the Pareto front of the mean changes both the range and the shape, rather than simply shifts in the Pareto space. The Pareto front of the means moves further towards the feasible region (or away from the utopia point [15]) with a decreasing value of  $\lambda$  (i.e., with more emphasis on the standard deviation), which indicates that when the robustness of the objectives increases, the performances must be sacrificed (i.e., a worse fatigue performance will be obtained for the same mass or vice versa). Besides, the longest fatigue life of the Pareto solutions would be reduced when increasing the robustness of the objectives.

Third, when  $\lambda$  has a very small value (for example  $\lambda = 0.01$ ), the Pareto front would be limited in the bottom right corner for the mean (Fig. 6a) and the bottom left corner for the standard deviation (Fig. 6b). Due to further improvement of the robustness of the objective

**Table 11**  
Results of mean and standard deviation.

No.	$F_\mu$	$F_\sigma$	$M_\mu$	$M_\sigma$
1	4.12	0.0618	24.79	0.3178
2	4.75	0.0974	28.93	0.3708
3	4.74	0.0964	28.31	0.3630
4	4.53	0.0888	26.05	0.3340
5	4.11	0.0947	20.68	0.2651
6	3.72	0.0512	18.64	0.2390
7	4.63	0.0921	27.17	0.3484
8	3.42	0.0644	18.96	0.2431
9	4.31	0.0919	23.40	0.3000
10	4.31	0.0680	25.35	0.3249
11	4.12	0.0956	22.82	0.2926
12	3.78	0.0759	19.26	0.2470
13	4.23	0.0849	24.91	0.3194
14	4.38	0.0842	24.37	0.3125
15	4.04	0.0853	21.88	0.2805
16	3.46	0.0710	17.45	0.2237
17	4.56	0.0898	26.01	0.3335
18	3.32	0.0629	18.12	0.2323
19	3.99	0.0787	20.09	0.2576
20	4.35	0.0899	25.63	0.3286
21	3.78	0.0655	19.27	0.2471
22	3.94	0.0642	22.52	0.2888
23	3.70	0.0734	20.98	0.2689
24	4.54	0.0935	26.50	0.3397
25	4.57	0.0736	27.65	0.3544
26	4.41	0.0919	23.57	0.3022
27	4.69	0.0952	28.63	0.3671
28	4.09	0.0744	21.83	0.2798
29	4.23	0.1006	22.56	0.2892
30	3.99	0.0589	21.94	0.2812
31	4.85	0.1036	30.02	0.3848
32	3.85	0.0660	21.76	0.2790
33	4.02	0.0581	22.53	0.2889
34	4.50	0.0905	25.21	0.3232
35	3.24	0.0636	16.86	0.2162

**Table 12**  
Accuracy assessment of DSMs.

DSM	Response	$R^2$	RAAE	RMAE
DPRS	$F_\mu$	0.9536	0.2006	0.2821
	$F_\sigma$	0.7761	0.4212	0.6727
DKRG	$F_\mu$	<b>0.9980</b>	<b>0.0374</b>	<b>0.0737</b>
	$F_\sigma$	<b>0.9530</b>	<b>0.1775</b>	<b>0.3808</b>
DRBF	$F_\mu$	0.9963	0.0586	0.0742
	$F_\sigma$	0.6299	0.4276	1.2603

functions, the mean of fatigue life becomes the worst of these three stages whilst that of the mass is the smallest. This implies that the robustness and performance of the fatigue durability conflict with each other, and thus a proper trade-off between them should be made. Furthermore, unlike for the first stage, not only the means but also the standard deviations of the objective functions conflict with each other as indicated in Fig. 6b.

In practical applications, a large value for  $\lambda$  should be utilized if emphasizing the nominal performances, while a small value for  $\lambda$  should be selected if emphasizing the robustness of the performances. To explain the effect of the proposed method, we select an optimum from the Pareto front obtained with  $\lambda = 0.05$  in this study, as signified with a red circle in Figs. 6a and b. Table 13 compares the optimal and baseline designs. It was found that the optimized design improves the fatigue life of truck cab, and simultaneously reduces the mass noticeably. Moreover, both the standard deviations of the fatigue life and mass decrease, which means that the objectives become more robust with the presence of the uncertainties.

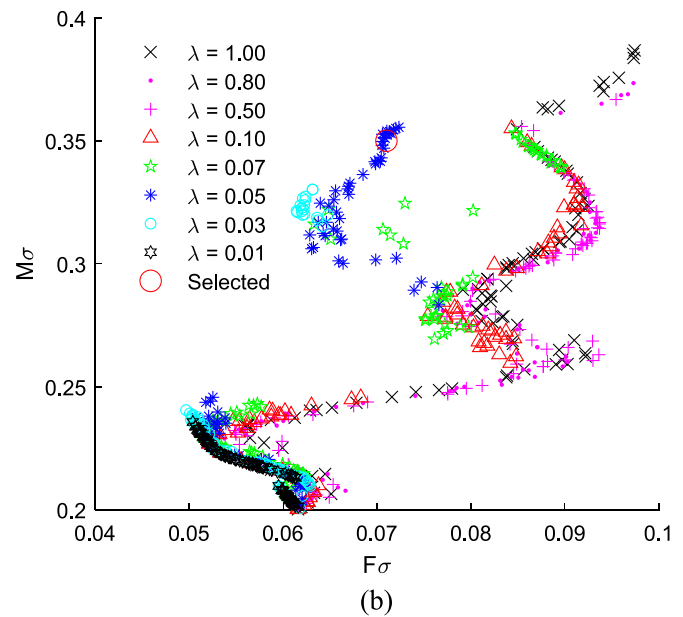
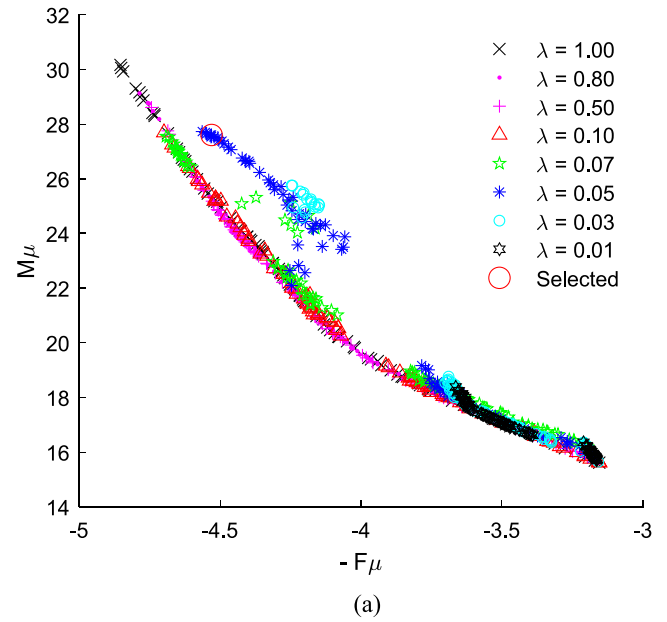


Fig. 6. Pareto fronts of the mean (a) and standard deviation (b) of the objectives. (For interpretation of the references to color in this figure legend, the reader is referred to the web version of this article.)

#### 4.4. Final design selection and comparison study

In engineering application, the Pareto provides a set of non-dominant results and are not satisfied in all cases. Thus a further analysis is needed to select the final optimal design from the obtained results. However, the obtained solutions from Pareto fronts can be compared by different MCDM methods, TOPSIS, WPM, and WSM [78]. Generally speaking, the objectives of optimization are measured with different units and these values need to be normalized to be comparable before the decision-making step. Thus, different normalization formulations (Linear, vector, and Linear max–min (LMM) [78]) can result in different values and consequently affect the solutions from MCDM.

In this study, the final designs selected by the three MCDM methods and three normalization techniques are compared as shown in Fig. 8, which are obtained from the Pareto front for  $\lambda = 0.05$ . It can be seen

**Table 13**  
Comparison of baseline and optimized designs of the truck cab.

Description		Baseline	Optimized	
			DSM	CAE simulation
Design variables	$x_1$	1.5 mm	2.00 mm	
	$x_2$	1.5 mm	0.85 mm	
	$x_3$	1.5 mm	0.92 mm	
	$x_4$	1.5 mm	0.70 mm	
Fatigue life (log)	$F_\mu$	4.45	4.53	4.49
	$F_\sigma$	0.076	0.071	0.070
Mass	$M_\mu$	33.46 kg	27.60 kg	27.60 kg
	$M_\sigma$	0.43 kg	0.35 kg	0.35 kg

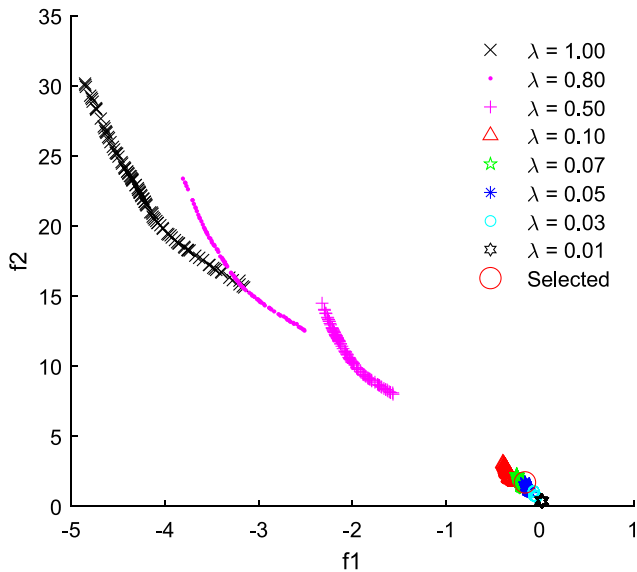


Fig. 7. Pareto fronts of  $f_1$  and  $f_2$ .

that the final design from the linear-based WSM method is the same as that from the Vector-based TOPSIS method. The final design from WPM is the same as that from the vector-based TOPSIS method. For

the linear, vector, and LMM normalization methods, the WSM decision-making method results in similar results. On the other hand, the TOPSIS obtained comparatively different results due to three normalizations. It shows that the normalization method has more effect on TOPSIS than the WSM method.

As shown in Table 14, the first-ranked solutions are selected to compare the effect of the normalization technique and MCDM methods on the result. Different from the TOPSIS and WSM method, WPM does not require to normalize the input value and only has one rank. The other rank is the results of employing TOPSIS and WSM methods due to normalization by Linear, vector, and LMM techniques. It was shown that optimal designs from Linear-based WSM, LMM-based WSM and Vector-based TOPSIS have the lease rank-sum for different methods and perform best. However, LMM-based TOPSIS has the largest rank-sum for different methods and performs worst for all cases. The comparison analysis emphasizes the importance of normalization and MCDM method selection in the optimal design selection process.

For the case study, as shown in Table 14, the top-ranked designs obtained based on WPM and WSM methods are generally similar, while that of the TOPSIS method are different. Besides, the TOPSIS method is relatively sensitive to a normalization method. For example, the TOPSIS top-rank design based on LMM normalization underperforms (rank 14 and 19) that of linear and vector normalization methods. Thus, the TOPSIS method has a low chance to select well-performed solutions compared to other MCDM and normalization methods and is not recommended to be employed alone to select the optimal solutions. When selecting optimal solutions from the Pareto fronts for different applications, the comparative study for different MCDM methods and

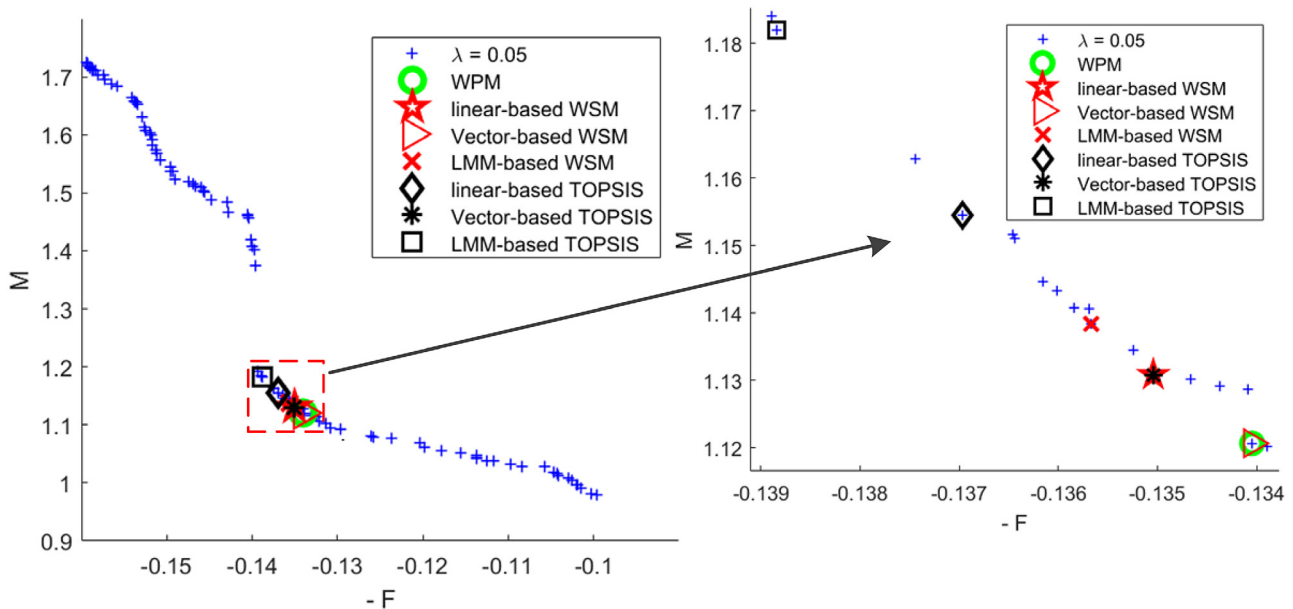


Fig. 8. Final design selections from three different normalization techniques within different MCDM methods.

**Table 14**  
Comparison of first-rank designs obtained from different normalization and MCDM methods.

Alternative I.Ds	Ranked by WPM	Ranked by WSM due to normalization by			Ranked by TOPSIS due to normalization by			Rank-sum for different methods
	Rank	Linear	Vector	LMM	Linear	Vector	LMM	
49	1	2	1	10	12	7	16	49
27	4	1	2	3	6	1	13	30
98	8	3	4	1	2	2	10	30
54	19	10	13	2	1	9	2	56
10	23	20	22	14	14	19	1	113

different normalization schemes in this study is recommended to be utilized for engineers.

## 5. Concluding remarks

To obtain robust designs considering uncertainty factors, the design problem of a truck cab was expressed as a multi-objective robust optimization problem aiming to minimize mass and maximize durability. To address the uncertainty and multi-objective optimization issues, the Taguchi parameter design, dual surrogate model method, and multi-objective particle swarm optimization (MOPSO) algorithm were integrated for obtaining a non-deterministic optimum. Taguchi parameter design was used to reduce the size and dimension of the design space, thereby simplifying the subsequent optimization. In this study, three different dual surrogate models, namely dual polynomial response surface, dual radial basis function models, and dual Kriging, were utilized to fit the mean and standard deviation of the mass and the log of fatigue life. Based on a comparative study, the dual Kriging was selected as the most accurate dual surrogate model in this case. MOPSO was then used to search the design space for the robust Pareto fronts. The influence of the weight factor on the Pareto front was investigated to provide some insightful information. Finally, the selected optimal solution from MORDO could increase fatigue life, reduce vehicle mass, and significantly improved the design robustness. To selecting an optimal design from the Pareto front, a comparison study of different normalization techniques introduced to different MCDM methods is recommended.

According to the numerical studies in this paper, the uncertainty in material properties has a large effect on fatigue performance. In the optimization process, although the prediction error is another important source of uncertainty, this is beyond the scope of this study. In future work, more focus is required to investigate the effects of the prediction error on fatigue performance optimization.

## Declaration of competing interest

The authors declare that they have no known competing financial interests or personal relationships that could have appeared to influence the work reported in this paper.

## Acknowledgments

This work was supported by The National Natural Science Foundation of China (51805123), Scientific Research Foundation of Hainan University, China (KYQD(ZR)1874), Hainan Provincial Natural Science Foundation of China (520RC538), The General Program of Natural Science Foundation of Hainan, China (517019), and Scientific Research Projects of Higher Education Institutions in Hainan Province, China (Hnky2018-8).

## References

- [1] H. Bayrakceken, S. Tasgetiren, I. Yavuz, Two cases of failure in the power transmission system on vehicles: A universal joint yoke and a drive shaft, *Eng. Fail. Anal.* 14 (4) (2007) 716–724.
- [2] D. Colombo, M. Gobbi, G. Mastinu, M. Pennati, Analysis of an unusual McPherson suspension failure, *Eng. Fail. Anal.* 16 (3) (2009) 1000–1010.
- [3] E.S. Palma, C.L. Petracconi, S.E. Ferreira, Fatigue behavior analysis of a rear tow hook pin of a passenger vehicle, *Eng. Fail. Anal.* 16 (7) (2009) 2408–2416.
- [4] V. Veloso, H.S. Magalhaes, G.I. Bicalho, E.S. Palma, Failure investigation and stress analysis of a longitudinal stringer of an automobile chassis, *Eng. Fail. Anal.* 16 (5) (2009) 1696–1702.
- [5] B.Y. He, S.X. Wang, F. Gao, Failure analysis of an automobile damper spring tower, *Eng. Fail. Anal.* 17 (2) (2010) 498–505.
- [6] Y.L. Hsu, M.S. Hsu, Weight reduction of aluminum disc wheels under fatigue constraints using a sequential neural network approximation method, *Comput. Ind. 46* (2) (2001) 167–179.
- [7] B.J. Kang, H.C. Sin, J.H. Kim, Optimal shape design of the front wheel lower control arm considering dynamic effects, *Int. J. Automot. Technol.* 8 (3) (2007) 309–317.
- [8] M. Mrzyglod, A.P. Zielinski, Parametric structural optimization with respect to the multiaxial high-cycle fatigue criterion, *Struct. Multidiscip. Optim.* 33 (2) (2007) 161–171.
- [9] Z. Ping, H. Jun, M. Jin, Fatigue life analysis of the autobody in a sports utility vehicle and its improvement using the homogenization method, *Proc. Inst. Mech. Eng. D* 222 (D12) (2008) 2291–2305.
- [10] A.H. Adl, M.S. Panahi, Multi-objective optimal design of a passenger car's body, *ASME Conf. Proc.* 2010 (49170) (2010) 277–286.
- [11] N. Kaya, I. Karen, F. Ozturk, Re-design of a failed clutch fork using topology and shape optimisation by the response surface method, *Mater. Des.* 31 (6) (2010) 3008–3014.
- [12] J.K. Kim, Y.J. Kim, W.H. Yang, Y.C. Park, K.H. Lee, Structural design of an outer tie rod for a passenger car, *Int. J. Automot. Technol.* 12 (3) (2011) 375–381.
- [13] X.G. Song, J.H. Jung, H.J. Son, J.H. Park, K.H. Lee, Y.C. Park, Metamodel-based optimization of a control arm considering strength and durability performance, *Comput. Math. Appl.* 60 (4) (2010) 976–980.
- [14] G.Y. Sun, G.Y. Li, Z.H. Gong, X.Y. Cui, X.J. Yang, Q. Li, Multiobjective robust optimization method for drawbead design in sheet metal forming, *Mater. Des.* 31 (4) (2010) 1917–1929.
- [15] G.Y. Sun, G.Y. Li, S.W. Zhou, H.Z. Li, S.J. Hou, Q. Li, Crashworthiness design of vehicle by using multiobjective robust optimization, *Struct. Multidiscip. Optim.* 44 (1) (2011) 99–110.
- [16] M.L. Boessio, I.B. Morsch, A.M. Awruch, Fatigue lifetime estimation of commercial vehicles, *J. Sound Vib.* 291 (1–2) (2006) 169–191.
- [17] R. d'Ippolito, S. Donderst, M. Hack, G. Van der Linden, D. Vandepitte, D. Moens, Reliability-based design of a slot-track fatigue life using mesh morphing technology, *AIAA J.* 46 (1) (2008) 154–165.
- [18] R. d'Ippolito, M. Hack, S. Donders, L. Hermans, N. Tzannetakis, D. Vandepitte, Improving the fatigue life of a vehicle knuckle with a reliability-based design optimization approach, *J. Statist. Plann. Inference* 139 (5) (2009) 1619–1632.
- [19] C.Y. Song, J. Lee, Reliability-based design optimization of knuckle component using conservative method of moving least squares meta-models, *Probabilistic Eng. Mech.* 26 (2) (2011) 364–379.
- [20] F. Li, G.W. Meng, L.R. Sha, L.M. Zhou, Robust optimization design for fatigue life, *Finite Elem. Anal. Des.* 47 (10) (2011) 1186–1190.
- [21] M. McDonald, M. Heller, Robust shape optimization of notches for fatigue-life extension, *Struct. Multidiscip. Optim.* 28 (1) (2004) 55–68.
- [22] T.G. Ritto, C. Soize, R. Sampaio, Robust optimization of the rate of penetration of a drill-string using a stochastic nonlinear dynamical model, *Comput. Mech.* 45 (5) (2010) 415–427.
- [23] N. Qiu, Y. Gao, J. Fang, G. Sun, Q. Li, N.H. Kim, Crashworthiness optimization with uncertainty from surrogate model and numerical error, *Thin-Walled Struct.* 129 (2018) 457–472.
- [24] Q. Zhou, Y. Wang, S.-K. Choi, P. Jiang, X. Shao, J. Hu, L. Shu, A robust optimization approach based on multi-fidelity metamodel, *Struct. Multidiscip. Optim.* 57 (2) (2017) 775–797.
- [25] M. Ouisse, S. Cogan, Robust design of spot welds in automotive structures: A decision-making methodology, *Mech. Syst. Signal Process.* 24 (4) (2010) 1172–1190.
- [26] M.L. Bouazizi, S. Ghanmi, N. Bouhaddi, Multi-objective optimization in dynamics of the structures with nonlinear behavior: Contributions of the metamodels, *Finite Elem. Anal. Des.* 45 (10) (2009) 612–623.
- [27] J.R. Cho, J.H. Lee, K.M. Jeong, K.W. Kim, Optimum design of run-flat tire insert rubber by genetic algorithm, *Finite Elem. Anal. Des.* 52 (2012) 60–70.

- [28] X.T. Liao, Q. Li, X.J. Yang, W.G. Zhang, W. Li, Multiobjective optimization for crash safety design of vehicles using stepwise regression model, *Struct. Multidiscip. Optim.* 35 (6) (2008) 561–569.
- [29] K.Y. Benyounis, A.G. Olabi, Optimization of different welding processes using statistical and numerical approaches – A reference guide, *Adv. Eng. Softw.* 39 (6) (2008) 483–496.
- [30] M. Kapsiz, M. Durat, F. Ficici, Friction and wear studies between cylinder liner and piston ring pair using Taguchi design method, *Adv. Eng. Softw.* 42 (8) (2011) 595–603.
- [31] G.I. Taguchi, *Introduction to Quality Engineering: Designing Quality Into Products and Processes*, Asian Productivity Organization, The Organization, Tokyo, 1986.
- [32] İ. Karen, A.R. Yildiz, N. Kaya, N. Öztürk, F. Öztürk, Hybrid approach for genetic algorithm and Taguchi's method based design optimization in the automotive industry, *Int. J. Prod. Res.* 44 (22) (2006) 4897–4914.
- [33] A. Yildiz, N. Öztürk, N. Kaya, F. Öztürk, Hybrid multi-objective shape design optimization using Taguchi's method and genetic algorithm, *Struct. Multidiscip. Optim.* 34 (4) (2007) 317–332.
- [34] W.J. Roux, N. Stander, R.T. Haftka, Response surface approximations for structural optimization, *Internat. J. Numer. Methods Engrg.* 42 (3) (1998) 517–534.
- [35] S. Bae, N.H. Kim, S.-g. Jang, Reliability-based design optimization under sampling uncertainty: Shifting design versus shaping uncertainty, *Struct. Multidiscip. Optim.* 57 (5) (2018) 1845–1855.
- [36] J. Fang, G. Sun, N. Qiu, N.H. Kim, Q. Li, On design optimization for structural crashworthiness and its state of the art, *Struct. Multidiscip. Optim.* 55 (3) (2016) 1091–1119.
- [37] J. Fang, Y. Gao, G. Sun, Q. Li, Multiobjective reliability-based optimization for design of a vehicle door, *Finite Elem. Anal. Des.* 67 (2013) 13–21.
- [38] N. Zabarar, S. Ganapathysubramanian, Q. Li, A continuum sensitivity method for the design of multi-stage metal forming processes, *Int. J. Mech. Sci.* 45 (2) (2003) 325–358.
- [39] O. Yeniay, R. Unal, R.A. Lepsch, Using dual response surfaces to reduce variability in launch vehicle design: A case study, *Reliab. Eng. Syst. Saf.* 91 (4) (2006) 407–412.
- [40] A.B. Shaibu, B.R. Cho, Another view of dual response surface modeling and optimization in robust parameter design, *Int. J. Adv. Manuf. Technol.* 41 (7–8) (2009) 631–641.
- [41] Y.Q. Li, Z.S. Cui, X.Y. Ruan, D.J. Zhang, CAE-based six sigma robust optimization for deep-drawing process of sheet metal, *Int. J. Adv. Manuf. Technol.* 30 (7–8) (2006) 631–637.
- [42] G.M. Quesada, E. Del Castillo, A dual-response approach to the multivariate robust parameter design problem, *Technometrics* 46 (2) (2004) 176–187.
- [43] W. Wang, W.H. Fan, T.Q. Chang, Y.M. Yuan, Robust collaborative optimization method based on dual-response surface, *Chin. J. Mech. Eng.* 22 (2) (2009) 169–176.
- [44] R. Jin, W. Chen, T.W. Simpson, Comparative studies of metamodelling techniques under multiple modelling criteria, *Struct. Multidiscip. Optim.* 23 (1) (2001) 1–13.
- [45] J. Fang, N. Qiu, X. An, F. Xiong, G. Sun, Q. Li, Crashworthiness design of a steel-aluminum hybrid rail using multi-response objective-oriented sequential optimization, *Adv. Eng. Softw.* 112 (2017) 192–199.
- [46] N. Qiu, Y. Gao, J. Fang, Z. Feng, G. Sun, Q. Li, Theoretical prediction and optimization of multi-cell hexagonal tubes under axial crashing, *Thin-Walled Struct.* 102 (2016) 111–121.
- [47] N. Qiu, Y. Gao, J. Fang, Z. Feng, G. Sun, Q. Li, Crashworthiness analysis and design of multi-cell hexagonal columns under multiple loading cases, *Finite Elem. Anal. Des.* 104 (2015) 89–101.
- [48] J. Fang, Y. Gao, G. Sun, N. Qiu, Q. Li, On design of multi-cell tubes under axial and oblique impact loads, *Thin-Walled Struct.* 95 (2015) 115–126.
- [49] S. Lee, J.H. Kim, An adaptive importance sampling method with a Kriging metamodel to calculate failure probability, *J. Mech. Sci. Technol.* 31 (12) (2017) 5769–5778.
- [50] H. Dong, B. Song, P. Wang, S. Huang, A kind of balance between exploitation and exploration on kriging for global optimization of expensive functions, *J. Mech. Sci. Technol.* 29 (5) (2015) 2121–2133.
- [51] S. Chen, T. Shi, D. Wang, J. Chen, Multi-objective optimization of the vehicle ride comfort based on Kriging approximate model and NSGA-II, *J. Mech. Sci. Technol.* 29 (3) (2015) 1007–1018.
- [52] G.Y. Sun, G.Y. Li, Q. Li, Variable fidelity design based surrogate and artificial bee colony algorithm for sheet metal forming process, *Finite Elem. Anal. Des.* 59 (2012) 76–90.
- [53] M. Buhmann, Radial basis functions: Theory and implementations, *Radial Basis Funct.* 12 (2003).
- [54] X. Gu, G. Sun, G. Li, L. Mao, Q. Li, A comparative study on multiobjective reliable and robust optimization for crashworthiness design of vehicle structure, *Struct. Multidiscip. Optim.* 48 (3) (2013) 669–684.
- [55] X. Song, G. Sun, G. Li, W. Gao, Q. Li, Crashworthiness optimization of foam-filled tapered thin-walled structure using multiple surrogate models, *Struct. Multidiscip. Optim.* 47 (2) (2012) 221–231.
- [56] H. Hamad, A. Al-Smadi, Space partitioning in engineering design via metamodel acceptance score distribution, *Eng. Comput.* 23 (3) (2007) 175–185.
- [57] G.Y. Sun, G.Y. Li, Z.H. Gong, G.Q. He, Q. Li, Radial basis functional model for multi-objective sheet metal forming optimization, *Eng. Optim.* 43 (12) (2011) 1351–1366.
- [58] J. Kennedy, R. Eberhart, Particle swarm optimization, in: *Neural Networks, 1995. Proceedings. IEEE International Conference on*, vol. 4, 1995, pp. 1942–1948.
- [59] X.T. Liao, Q. Li, X.J. Yang, W. Li, W.G. Zhang, A two-stage multi-objective optimization of vehicle crashworthiness under frontal impact, *Int. J. Crashworthiness* 13 (3) (2008) 279–288.
- [60] G. Sun, H. Zhang, J. Fang, G. Li, Q. Li, Multi-objective and multi-case reliability-based design optimization for tailor rolled blank (TRB) structures, *Struct. Multidiscip. Optim.* 55 (5) (2016) 1899–1916.
- [61] C.R. Raquel, P.C. Naval, An effective use of crowding distance in multiobjective particle swarm optimization, in: *GECCO 2005: Genetic and Evolutionary Computation Conference*, vols. 1 and 2, 2005, pp. 257–264.
- [62] C.A.C. Coello, G.T. Pulido, M.S. Lechuga, Handling multiple objectives with particle swarm optimization, *IEEE Trans. Evol. Comput.* 8 (3) (2004) 256–279.
- [63] D.S. Liu, K.C. Tan, C.K. Goh, W.K. Ho, A multiobjective memetic algorithm based on particle swarm optimization, *IEEE Trans. Syst. Man Cybern. B* 37 (1) (2007) 42–50.
- [64] Q. Gao, L. Wang, Y. Wang, F. Guo, Z. Zhang, Optimization of foam-filled double ellipse tubes under multiple loading cases, *Adv. Eng. Softw.* 99 (2016) 27–35.
- [65] A. Kaveh, K. Laknejadi, A new multi-swarm multi-objective optimization method for structural design, *Adv. Eng. Softw.* 58 (2013) 54–69.
- [66] Z. Xiao, J. Fang, G. Sun, Q. Li, Crashworthiness design for functionally graded foam-filled bumper beam, *Adv. Eng. Softw.* 85 (2015) 81–95.
- [67] S. Mirjalili, A.H. Gandomi, S.Z. Mirjalili, S. Saremi, H. Faris, S.M. Mirjalili, Salp swarm algorithm: A bio-inspired optimizer for engineering design problems, *Adv. Eng. Softw.* (2017).
- [68] N. Qiu, Y. Gao, J. Fang, G. Sun, N.H. Kim, Topological design of multi-cell hexagonal tubes under axial and lateral loading cases using a modified particle swarm algorithm, *Appl. Math. Model.* 53 (2018) 567–583.
- [69] J. Fang, Y. Gao, G. Sun, G. Zheng, Q. Li, Dynamic crashing behavior of new extrudable multi-cell tubes with a functionally graded thickness, *Int. J. Mech. Sci.* 103 (2015) 63–73.
- [70] A. Majumder, Process parameter optimization during EDM of AISI 316 LN stainless steel by using fuzzy based multi-objective PSO, *J. Mech. Sci. Technol.* 27 (7) (2013) 2143–2151.
- [71] G. Sun, G. Li, S. Hou, S. Zhou, W. Li, Q. Li, Crashworthiness design for functionally graded foam-filled thin-walled structures, *Mater. Sci. Eng. A* 527 (7–8) (2010) 1911–1919.
- [72] J. Fang, Y. Gao, G. Sun, C. Xu, Q. Li, Fatigue optimization with combined ensembles of surrogate modeling for a truck cab, *J. Mech. Sci. Technol.* 28 (11) (2015) 4641–4649.
- [73] K.S. Lee, J.H. Song, Estimation methods for strain-life fatigue properties from hardness, *Int. J. Fatigue* 28 (4) (2006) 386–400.
- [74] M.A. Meggiolaro, J.T.P. Castro, Statistical evaluation of strain-life fatigue crack initiation predictions, *Int. J. Fatigue* 26 (5) (2004) 463–476.
- [75] A. Bäuml, T. Seeger, C. Boller, *Materials Data for Cyclic Loading: Supplement 1*, Elsevier, 1990.
- [76] *ASM International. Handbook Committee, ASM Handbook, tenth ed., ASM International, Materials Park, OH, 1990.*
- [77] R.J. Yang, N. Wang, C.H. Tho, J.P. Bobineau, Metamodeling development for vehicle frontal impact simulation, *Trans. ASME, J. Mech. Des.* 127 (5) (2005) 1014–1020.
- [78] H. Jafaryganeh, M. Ventura, C. Guedes Soares, Effect of normalization techniques in multi-criteria decision-making methods for the design of ship internal layout from a Pareto optimal set, *Struct. Multidiscip. Optim.* 62 (4) (2020) 1849–1863.